

# Hot Reservoir Variable Conductance Heat Pipe with Advanced Fluid Management

Kuan-Lin Lee<sup>1</sup>, Calin Tarau<sup>2</sup>, Sanjay Adhikari<sup>3</sup> and William G. Anderson<sup>4</sup>  
*Advanced Cooling Technologies, Inc., Lancaster, PA, 17601*

Chirag Kharangate<sup>5</sup>, Cho-Ning Huang<sup>6</sup> and Yasuhiro Kamotani<sup>7</sup>  
*Case Western Reserve University, Cleveland, OH, 44106*

A hot reservoir variable conductance heat pipe (VCHP) can offer a significantly tighter passive thermal control than a regular VCHP with a cold-biased reservoir. This attribute makes the hot reservoir VCHP an ideal thermal management device for future planetary landers and rovers and especially for the moon where surviving of the lunar night is energetically challenging. Since the hot reservoir cannot be wicked, it becomes a challenge to properly manage the presence of working fluid within the reservoir. To ensure a long-duration operation of the hot reservoir VCHPs in reduced gravity and in microgravity, advanced fluid management strategies and features must to be developed. Advanced Cooling Technologies, Inc. (ACT) in collaboration with Case Western Reserve University (CWRU) is developing a reliable VCHP configuration under the NASA STTR program. The novel VCHP consists of a loop with well-engineered tubing configuration that would generate a momentum induced continuous flow within the device. This induced flow would provide continuous maintenance of the Non Condensable Gas (NCG) humidity in the reservoir as well as enable a much faster purging process (i.e., removal of moisture from the hot reservoir) if needed, significantly enhancing device's reliability. The development of hot reservoir VCHP with advanced fluid management features will be presented in this paper, including both numerical and experimental efforts.

## Nomenclature

|                  |   |  |
|------------------|---|--|
| $A_c$            | = | active condensation area   |
| $D_{12}$         | = | binary diffusion coefficient between vapor and Non Condensable Gas (NCG) |
| $g$              | = | gravity (9.81 m/s <sup>2</sup> )   |
| $h_{fg}$         | = | latent heat of evaporation   |
| $h_c$            | = | condensation heat transfer coefficient                                   |
| $L$              | = | total length of heat pipe section  |
| $L_c$            | = | heat pipe condenser length   |
| $\dot{m}_{cond}$ | = | vapor condensation rate  |
| $P$              | = | pressure   |
| $Q$              | = | heat load  |
| $R$              | = | internal radius of the heat pipe section                                 |
| $r$              | = | radial direction   |
| $T$              | = | temperatura  |
| $T_{sat}$        | = | saturated vapor temperature  |
| $T_{sink}$       | = | sink temperature   |
| $t$              | = | time   |
| $u_r$            | = | vapor velocity in radial direction                                       |
| $u_z$            | = | vapor velocity in axial direction  |
| $z$              | = | axial direction  |
| $\alpha$         | = | thermal diffusion coefficient of the vapor                               |

<sup>1</sup> R&D Engineer III, Advanced Cooling Technologies, Inc., 1046 New Holland Ave., Lancaster, PA 17601.

<sup>2</sup> Principal Engineer, Advanced Cooling Technologies, Inc., 1046 New Holland Ave., Lancaster, PA 17601

<sup>3</sup> R&D Engineer II, Advanced Cooling Technologies, Inc., 1046 New Holland Ave., Lancaster, PA 17601

<sup>4</sup> Chief Engineer, Advanced Cooling Technologies, Inc., 1046 New Holland Ave., Lancaster, PA 17601

<sup>5</sup> Assistant Professor, Case Western Reserve University, 10900 Euclid Ave., Cleveland, OH 44106

<sup>6</sup> Graduate Student, Case Western Reserve University, 10900 Euclid Ave., Cleveland, OH 44106

<sup>7</sup> Professor, Dept. Case Western Reserve University, 10900 Euclid Ave., Cleveland, OH 44106

|           |   |                                    |
|-----------|---|------------------------------------|
| $\phi$    | = | vapor concentration                |
| $\varphi$ | = | heat pipe titled angle             |
| $\rho$    | = | vapor density                      |
| $\mu$     | = | vapor dynamic viscosity            |
| HR        | = | Hot Reservoir                      |
| ID        | = | Inner Diameter                     |
| OD        | = | Outer Diameter                     |
| NCG       | = | Non Condensable Gas                |
| STTR      | = | Small Business Technology Transfer |
| VCHP      | = | Variable Conductance Heat Pipe     |

## I. Introduction

As NASA adventures back to the moon, spacecraft thermal designers are faced with the unprecedented challenge of surviving extended excursions in the cold and frigid environment of the lunar night, potentially using only resistive heating. Thermal management for the Moon is much more complicated than it is for near-Earth spacecraft and Mars Rovers, due to the 14-day long Lunar Night. Since many Lunar Landers and Rovers are solar-powered, batteries are required to provide survival power. Survival power must be minimized since providing 1 Watt over the 14-day long Lunar Night requires about 5 kg of extra solar cells and batteries. This can be done with a passive variable thermal link between the battery box and the radiator, which can be a Hot Reservoir Variable Conductance Heat Pipe (HR-VCHP).

A hot reservoir variable conductance heat pipe as Figure 1 shows, has a Non-condensable Gas (NCG) reservoir located near the evaporator and the reservoir temperature follows the evaporator. This will significantly improve the tightness of thermal control capability compared to a conventional cold-biased reservoir VCHP and it is fully passive (i.e., reservoir is heated by the payload waste heat). This technology has been developed and successfully demonstrated by Advanced Cooling Technologies, Inc. through analytical modeling and a series of ground testing (ref. 1,2 and 3). Most recently, an HR-VCHP prototype was tested on ISS as part of the APTx project in 2017 (ref.4), which showed that to ensure a reliable operation of HR-VCHP in space, advanced fluid management features are needed. This includes (1) prevention of working fluid condensing in the non-wicked reservoir and (2) fast removal of excessive working fluid (both vapor and liquid) from the reservoir or so call “reservoir purging” capability.

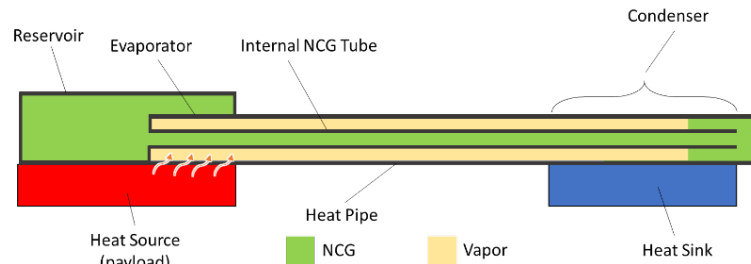


Figure 1. A hot reservoir VCHP with internal NCG tube and reservoir integrated with heat pipe evaporator

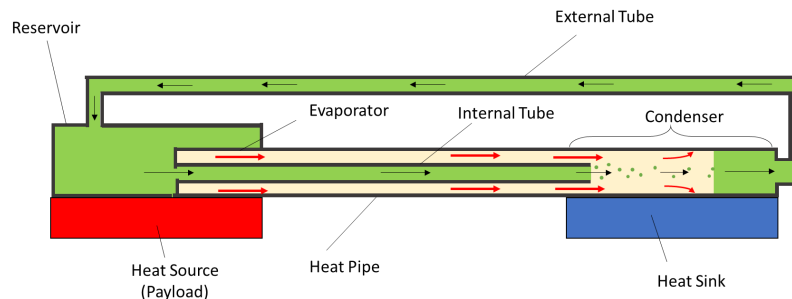


Figure 2. HR-VCHP with a loop configuration to improve fluid management (red arrows: primary vapor flow direction; black arrows: secondary flow)

To address this, ACT in collaboration with Case Western Reserve University (CWRU) performed a fundamental study on HR-VCHP and developed a new loop VCHP configuration (ref.5) as Figure 2 illustrated. The configuration consists of a warm reservoir (can be integrated or non-integrated), heat pipe sections, and two NCG links. One link is internal, coming out from the reservoir and going through the heat pipe section from the evaporator side. The second NCG link is external, connecting the end of the condenser with the reservoir. This advanced loop configuration would allow a secondary (NCG) fluid flow to be induced by the momentum of the primary vapor flow through the annular region of the heat pipe section. The secondary flow will travel along the loop in the favorable direction (reservoir-internal tube – condenser) and remove excessive vapor from the reservoir if exists. A detailed mechanism of flow generation within a VCHP loop was discussed in the previous paper (ref.5)

Even though the momentum induced flow (mostly NCG) is relatively weak (few cm/s) it would still be very beneficial to support a reliable operation of VCHP in microgravity due to the following aspects:

- During startup, this flow will condition the VCHP by transporting the NCG-vapor mixture from the reservoir to the condenser via the internal NCG tube. This will dehumidify the reservoir by bringing dryer NCG from the condenser via the external tube.
- The induced flow would be permanent during nominal operation. Therefore, the vapor concentration within the reservoir can be maintained at low (desired) values all the time.
- Based on the above-described mechanism, heating of the reservoir (to encourage purging) may be eliminated.

The loop concept and the existence of induced flow were successfully proven both theoretically (numerically) and experimentally in a Small Business Technology Transfer (STTR) phase I program. One major objective of the Phase II program is to understand the momentum induced flow through both modeling and testing and further maximize the flow rate through design optimization. This paper reports the status of the development of advanced HR-VCHP, including an experimental study and numerical analysis.

## II. Experimental study of Loop Hot Reservoir VCHP

### A. Description of Loop VCHP Experimental System

An experimental system to study momentum-induced flow within a loop VCHP was developed and it is shown in Figure 3. The heat pipe section (shown in transparent) has the dimensions of 1.59 cm Outer Diameter (OD), 0.58 mm wall thickness and 30.5 cm as total length. It is made of titanium. The external NCG loop tubing is 1.27 cm OD and 0.89 mm wall thickness. The evaporator is heated by a 10.2 cm heater block and the condenser sections are cooled by a chiller block with 10.2 cm length. Since the liquid return is not the focus of this study, this heat pipe is tested in a gravity-aided orientation with a tilted angle of 5°. The system has a non-integrated NCG reservoir and its temperature is maintained by electric heating to be higher than the evaporator during the test. Temperatures at various locations on the heat pipe system, system pressure, and secondary flow rate are measured. Calculated amounts of helium (NCG) and acetone (working fluid) were charged. The chiller block temperature is maintained by a constant temperature bath with a set point of 5°C.

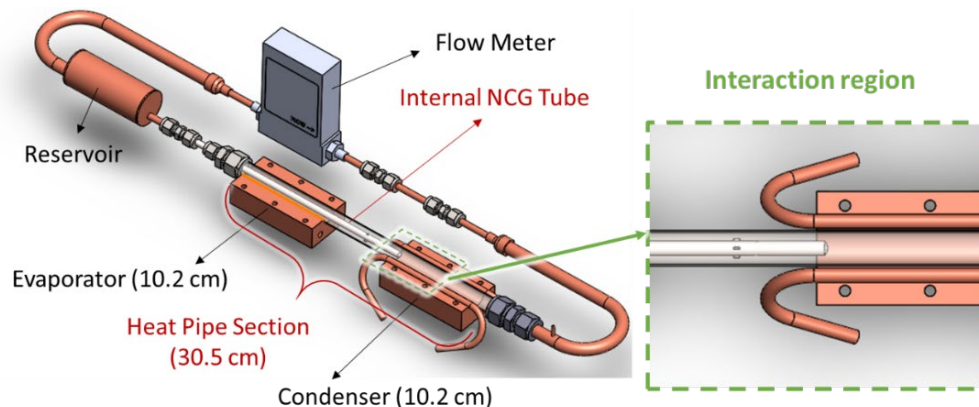
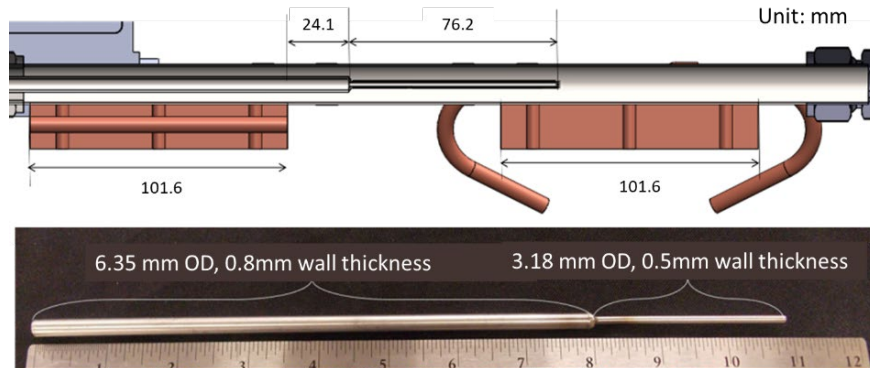
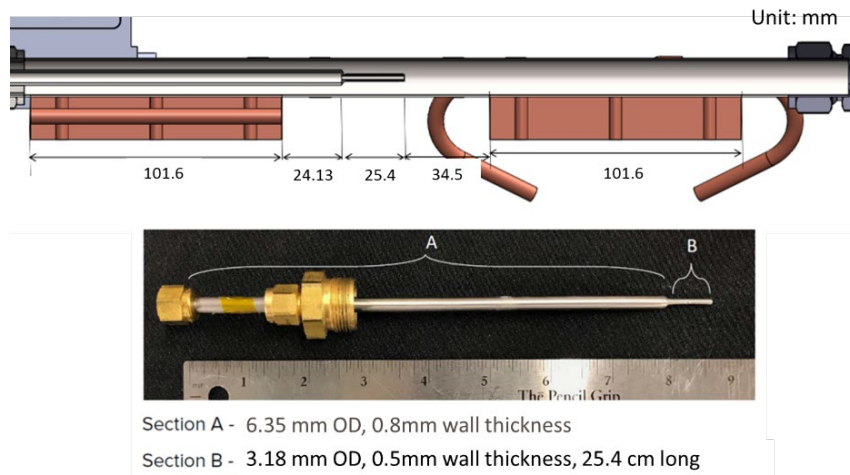


Figure 3 CAD model of the loop VCHP experimental system. The heat pipe section is shown in transparent to show the internal NCG tube

One key parameter to be studied for this experiment is the internal NCG tube design. Based on the theoretical study performed in Phase I, the momentum-induced flow heavily depends on the impact of the geometry of the NCG tube on the annular vapor flow (primary flow) as well as on the interaction between this primary flow and the NCG. The interaction region between the two species, vapor and NCG, is marked with a dashed green line, and it should be investigated in detail. Several internal NCG tubes with different geometries are fabricated and tested with this test apparatus. Figures 4 and 5 show two NCG tube designs. Both designs consist of two sections: a section with 0.64 cm OD and another section with 0.32 cm OD. The reason to have a reduced OD at the exit of the internal NCG tube is to mitigate the negative pressure gradient generated by flow expansion around the flow interaction region, which will be discussed in the modeling section below. NCG tube Design #2 is 5.08 cm shorter than Design #1 and therefore its outlet is located further away from the condenser, within the adiabatic section as illustrated in Figure 5.



**Figure 4. Internal NCG tube Design #1**

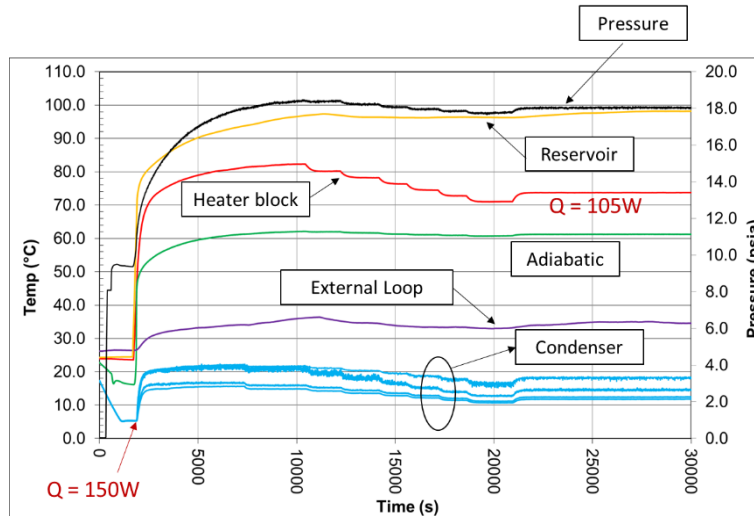


**Figure 5. Internal NCG tube Design #2**

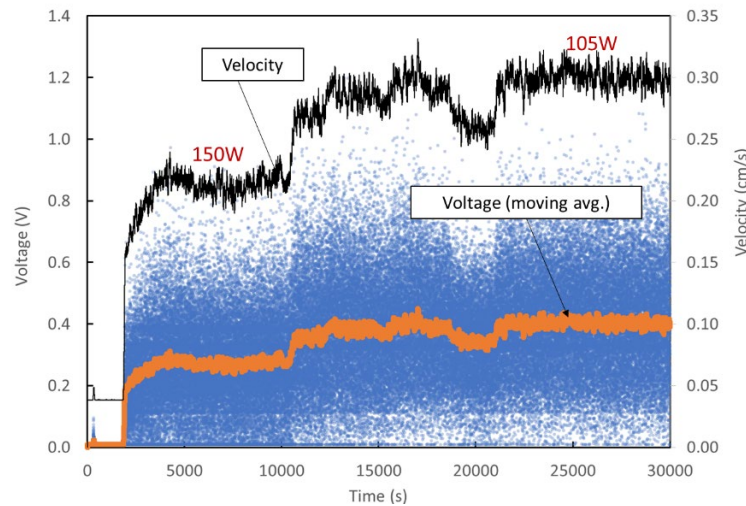
## B. Test results and discussion

Figure 6 shows the temperature and pressure (right axis) variations of the HR-VCHP with tube Design #1. The chiller temperature is maintained constant at 5°C. Reservoir temperature is maintained above evaporator temperature. The corresponding flow meter signal and induced flow velocity are shown in Figure 7. Blue dots are the actual voltage output and the orange line is the moving average. At  $t=2500$  sec, 150W of heat is applied to the evaporator. A strong voltage signal shows up in Figure 7, indicating that an NCG flow is induced, which is fluctuating with an amplitude of 0.3 volts. The source of flow oscillation can be the bubbling of working at the liquid puddle in the evaporator as the heat pipe is slightly tilted. Heat inputs are turned down from 150W to 90W from  $t = 10,000$  seconds. The trend of the flow signal (blue dots) moves upward and starts detaching from the bottom of the graph. This means that more flow signal in the positive direction is detected. At  $t = 20,000$  sec, constant power of 105W is applied for the remaining test. The moving average of the flow signal is around 0.4 volts. After conversion, the corresponding induced flow

velocity through a 0.635 cm OD tubing is shown as a black line in the same plot. With  $Q = 105\text{W}$ , the primary vapor flow can induce  $\sim 0.3\text{ cm/s}$  of secondary flow moving in a favorable direction. It can also be seen from Figure 6 that due to this induced flow, the vapor pressure and temperature (green line) of the heat pipe can be maintained at a constant value. Without flow, both the pressure and temperature of the system would keep increasing due to NCG diffusion from the reservoir into the condenser.



**Figure 6. Pressure and temperature variation of the VCHP loop with NCG tube #1. Heat inputs decrease from 150W to 100W and chiller temperature is at a constant of 5°C**



**Figure 7. Flowmeter voltage (left axis) and induced flow velocity (right axis) resulted from the testing of NCG tube Design #1. Blue dots: voltage readout; orange line: voltage moving average; black line: converted flow velocity**

Test results of Design #2 are shown in Figure 8 (temperature and pressure) and Figure 9 (flow signal and velocity). In this test, chiller block temperature is maintained at 5°C and the power is incrementally increased from 50W to 140W. The corresponding secondary flow velocity increases as the power increases. When  $Q = 140\text{W}$ , the induced flow velocity can reach  $\sim 0.54\text{ cm/s}$ . Compared to the test result of Design #1, which shows 0.25 cm/s of induced flow velocity with 150W of heat input (see Figure 7). Having a shorter internal NCG tube or increasing the distance between the NCG tube outlet and the condenser would result in a higher momentum-induced flow velocity within a VCHP. After this test, the NCG tube was machined and the wall thickness at the outlet was reduced from 0.5 mm to 0.31 mm (i.e., Inner diameter of NCG tube outlet was slightly increased). This tube design is called “Design #2B” and the test results are shown in Figure 10 and Figure 11. As the heat input increases from 80W to 170W, the flow velocity first

increases, reaches a maximum value at 0.55 cm/s, and then decreases to 0.30 cm/s. The maximum induced flow occurs at a power of around 140W.

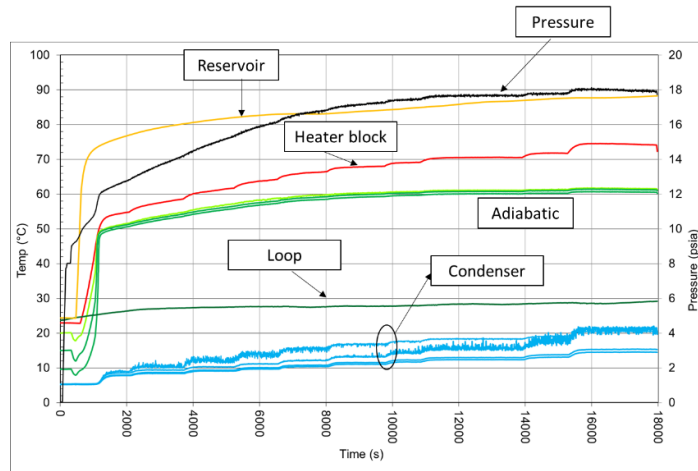


**Figure 8. Pressure and temperature variation of the VCHP loop with NCG tube #2. Heat input increases from 50W to 140W**

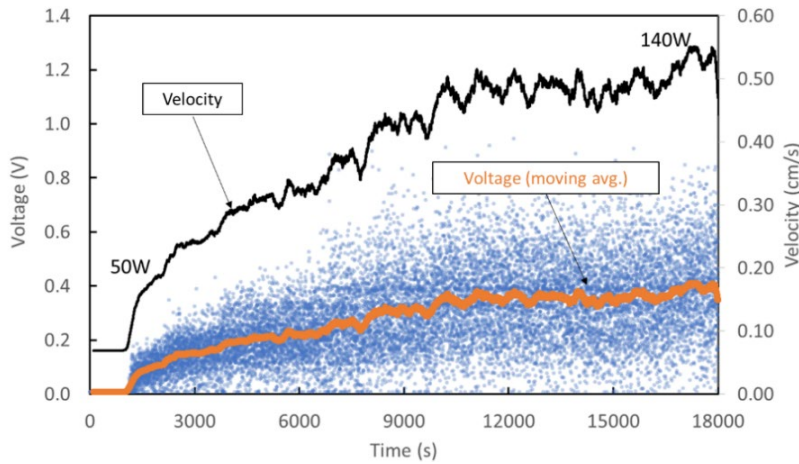


**Figure 9. Flow meter voltage (left axis) and velocity (right axis) resulted from the testing of NCG tube #2**

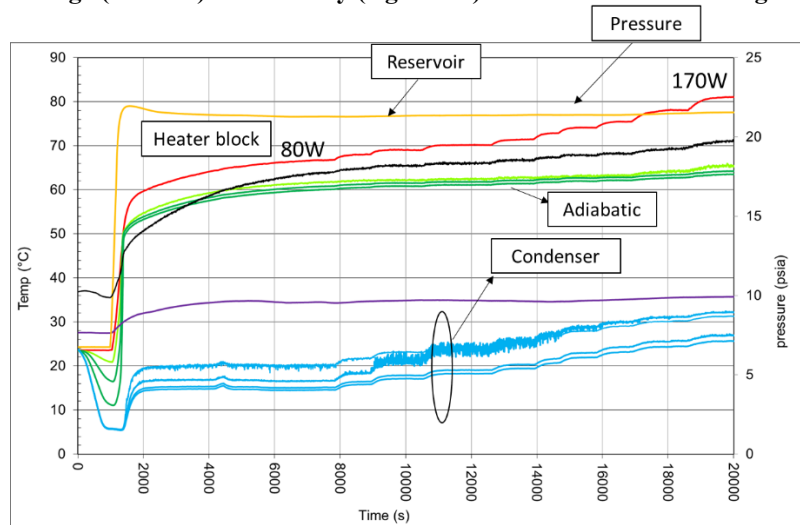


**Figure 10. Pressure and temperature variation of the VCHP loop with NCG tube #2B (thinner wall). Power increases from 80W to 170W**

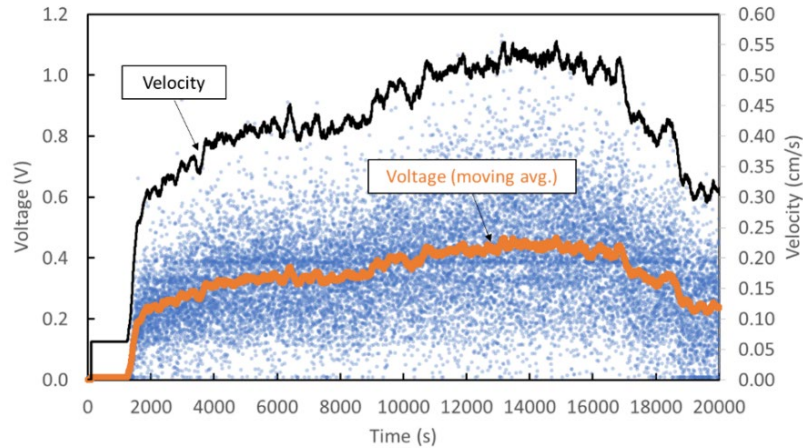


**Figure 11. Flow meter voltage (left axis) and induced flow velocity (right axis) resulted from the testing of NCG tube #2B**

Through this round of experimental study, it was observed that:

- (1) Momentum induced flow exists and its flow rate is resulted from vapor and NCG interaction
- (2) Reducing NCG tube outlet OD or increasing the annular area around the interaction region is favorable for flow generation
- (3) Keeping NCG tube outlet away from the condenser is favorable for flow generation
- (4) For certain NCG tube designs, there is an optimum heat input that can generate maximum induced flow velocity.

This could be explained by vapor flow deceleration at the NCG/vapor interaction region, which is illustrated in Figure 12. Vapor traveling through the annular region between inner and outer pipes in the adiabatic section has a high velocity and a static pressure of  $P_1$ . When the vapor flow passes around the outlet of NCG tube, the flow will decelerate due to two effects (1) sudden expansion of flow area (2) vapor condensation. Vapor flow will start separating from the internal tube and a wake will form at the tip of the NCG tube outlet as flow pattern shows in Figure 12. A vortex will be generated behind the NCG tube outlet. The size of the vortex primarily depends on the differences of back pressure ( $P_3$ ) and the lowest pressure point of the system, which is the outlet of NCG tube ( $P_2$ ). This vortex would discourage the development of the flow induced by the momentum exchange between vapor and NCG. By increasing the annular space between the inner and outer pipes, the area expansion ratio at the NCG outlet becomes milder and the negative impact to the momentum induced flow becomes smaller. Also keeping NCG tube outlet away from the condenser would mitigate the flow deceleration contributed from both flow area expansion and vapor condensation. This theory can also explain the existence of optimum power for flow maximization: increasing the heat input would result in a higher momentum of primary flow (vapor), which is good for secondary flow generation. However, higher heat input might result in a larger recirculation wake, which is unfavorable for flow generation. A Computational Fluid Dynamics (CFD) analysis was performed to further validate this hypothesis.

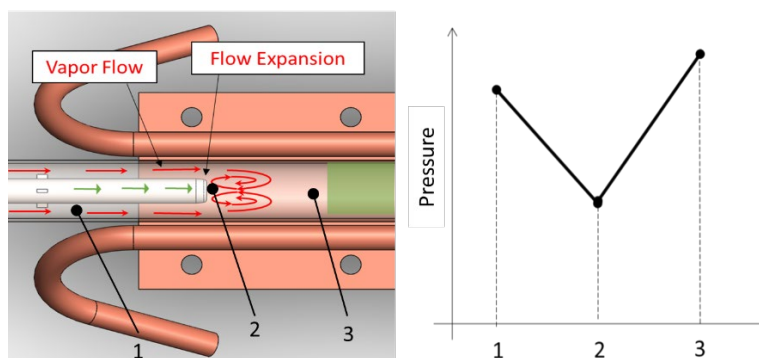


**Figure 12. Flow pattern and pressure distribution around the interaction region**

### III. Numerical Study of Loop HR-VCHP

This section presents a numerical scheme developed by Case Western Reserve University (CWRU) to theoretically study the momentum-induced flow within a VCHP with a loop configuration.

#### A. Numerical scheme to calculate vapor flow and pressure distribution in the heat pipe section

The computation domain is shown in Figure 13 (a) and (b), which contains the working fluid (acetone vapor) region, the solid wall region, and the NCG (helium) region. In the present CFD analysis, two velocity profiles at the end of the evaporator section are specified as a flow boundary condition. As shown in Figure 13(c), one profile is resulting from uniform evaporation and the other profile is for uniform flow. The former profile (dash line in Figure 13(c)) is mainly used in the present study when the vapor flow is considered to be laminar. The latter profile is considered to be caused by uniformly mixed flow in the evaporator, which occurs when the flow is turbulent and fully developed. Since the present model can only capture laminar flow, the uniform velocity distribution (solid line in Figure 13(c)) is only used to explain why the induced flow decreases as the heat input (and therefore the primary vapor flow Reynolds number) increases.

The flow motion within the VCHP loop is governed by continuity, momentum, energy, and diffusion equations (see appendix). The calculation flow chart is shown in Figure 14. First, a guessed location of the interface is used. Next, SIMPLER method is applied to calculate the velocity field, pressure field, temperature field, and concentration field in the computational domain. Finally, the match between the condensation heat transfer rate and the applied power is verified. If true, then the calculation is completed. If false, then the interface location is changed and another iteration will be applied until the difference between them is under the tolerance of 0.1%. It is assumed that there is no condensation happening in the NCG region to improve model stability. It was verified that the concentration of acetone beyond the front is only 0.15~0.2 and the mass flow rate from this region is very little compared to the vapor region. Therefore, the effect on flow and heat transfer should be insignificant.

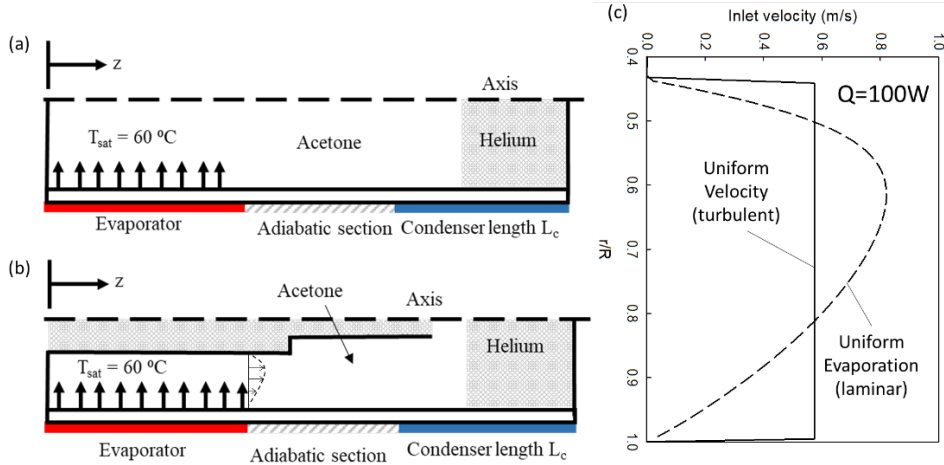


**Figure 13. (a) Computational domain for vapor velocity and pressure contour calculation in VCHP without internal NCG tube (b) Computational domain for vapor velocity and pressure contour calculation in VCHP with internal NCG tube (c) two vapor velocity profiles at the end of evaporator section.**

## B. Streamlines and pressure contours

Typical streamline patterns with uniform evaporation (parabolic velocity profile) are shown in Figure 15 with and without the internal NCG tube. Without the NCG pipe, the flow structure is relatively simple. In contrast, with the inner tube, the flow around the condenser is significantly altered. A recirculating flow (toroidal vortex flow) appears between the NCG tube outlet and the vapor-NCG interface. When the vapor flow approaches the condenser, it will lose its forward momentum due to vapor condensation. With an internal NCG tube, this deceleration process happens from the lower velocity near the tube wall because of the no-slip boundary condition. Consequently, the fluid near the centerline loses the forward momentum ahead of the faster-moving fluid in the middle, resulting in the appearance of the recirculating cell after the fluid departs from the centerline region. The appearance of the vortex flow alters the pressure distribution appreciably as shown in Figure 16. In both cases (with and without NCG tube), the average pressure decreases at first with increasing axial distance due to the friction. Once the flow gets into the condenser region, the pressure increases monotonically for the case without the NCG tube up to the vapor-NCG interface. With the NCG tube, the aforementioned recirculation vortex alters the pressure field appreciably. The net effect is that the pressure increase in the NCG region is smaller than in the case without the NCG tube. The flow in the external loop is induced by the difference between the pressure in the NCG region and the pressure at the NCG pipe outlet ( $\Delta P$ ). This pressure difference decreases significantly with the presence of an internal NCG tube.

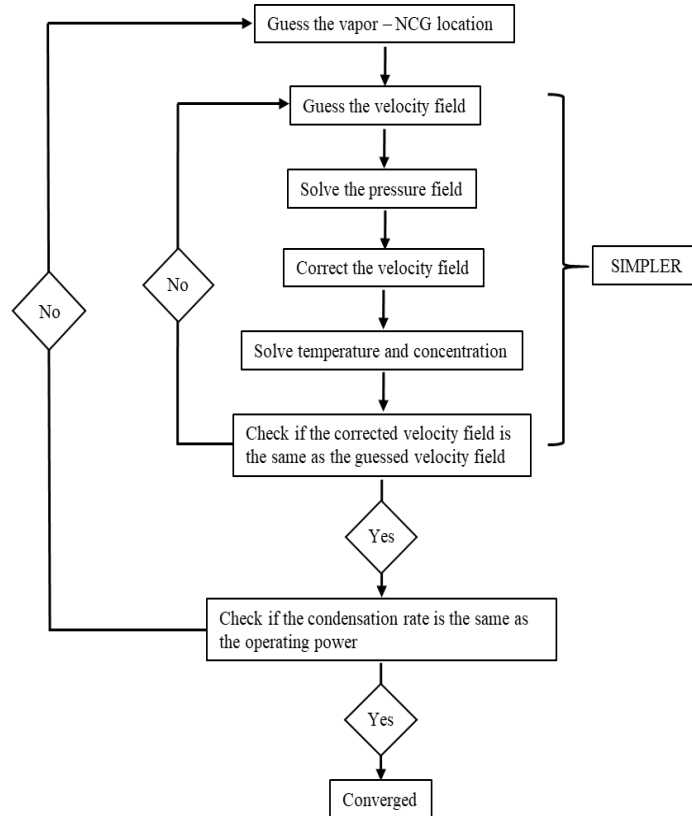


Figure 14 Iteration steps

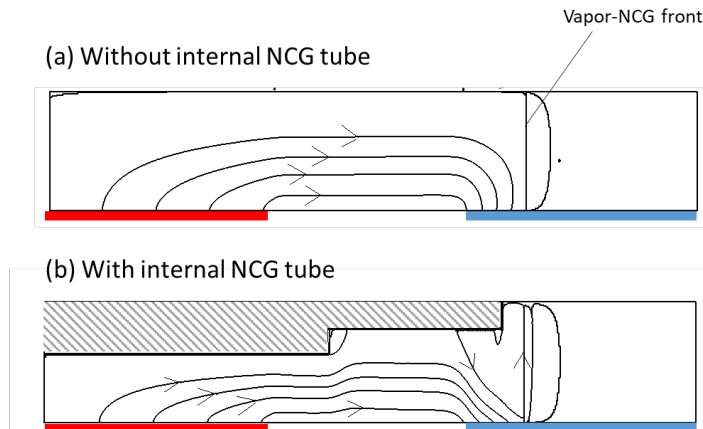
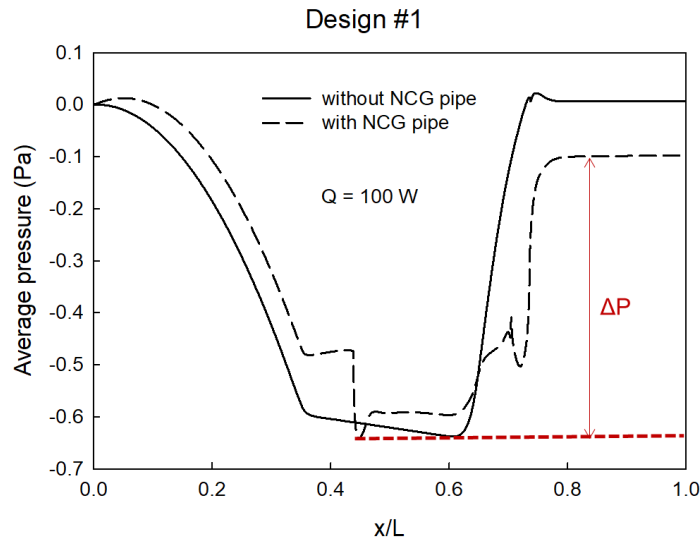


Figure 15. Streamline contours (a) without internal NCG tube (b) with internal NCG tube



**Figure 16. Axial pressure distribution with and without an internal NCG tube (Design #1).  $\Delta P$  between the outlet of the NCG tube and vapor-NCG interface at the condenser is the main driving force for the secondary flow**

#### IV. Results and Discussion

The predicted loop velocities are compared with the experimental data in Figure 17 for Design #1. As Figure 17(a) shows, the case where the flow boundary condition (velocity profile) is “with evaporator” over-predicts while when this is ‘uniform inlet flow’ under-predicts the experimental data. A close examination shows that there is an important difference between the CFD and the experimental results in terms of the location of the vapor-NCG interface. At  $Q = 100$  W, the predicted interface with the evaporator profile is located at 25% of the condenser section, while in the experiment, the interface is found to be located at about the mid-point of the condenser. Therefore, the condensation rate in the CFD simulation is reduced by 40 % so that the computed interface is located at the mid-point of the condenser for Design #1 and  $Q = 100$  W. The predicted loop velocities for the profile “with evaporator” are compared with the experimental data in Figure 17(b), which shows a good agreement between them up to about  $Q = 130$  W. Beyond this power, in the experiment, the loop velocity decreases with increasing power. Interestingly, the CFD solution does not converge beyond  $Q = 130$  W.

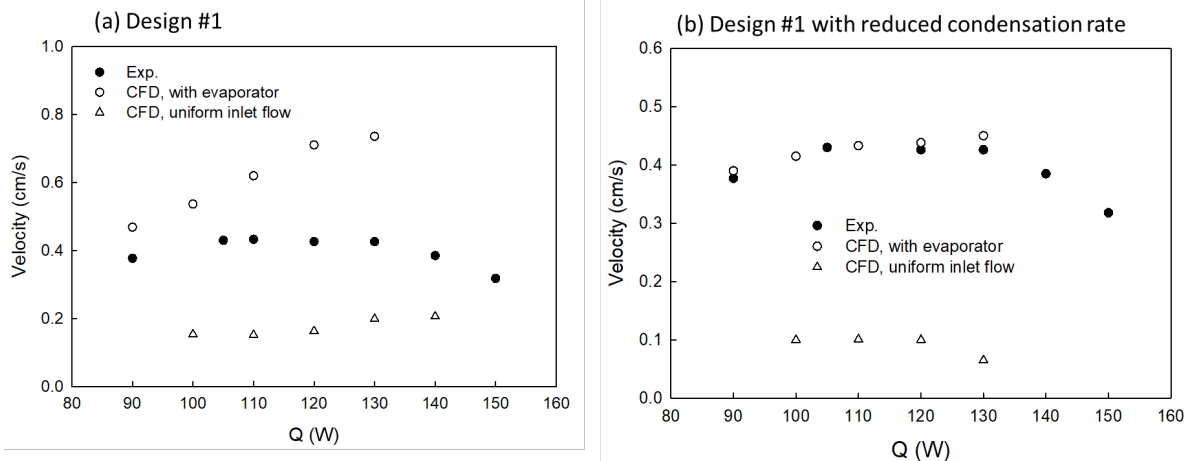


**Figure 17. Comparison of induced flow velocity between CFD simulation and experiment results for NCG tube Design #1 (a) before adjustment of the condensation rate (b) after adjustment of the condensation rate to match NCG-vapor front location**

The problem of not converging for high power as discussed in Figure 17 can be explained by the vapor flow Reynolds number. It can be shown that the Reynolds number is about 2,000 at  $Q = 130$  W so that the flow begins to deviate from laminar flow regime beyond this power. With this transition to turbulence, the axial velocity profile at the end of the evaporator section deviates from the uniform evaporation profile and becomes closer to the uniform velocity profile. Although the current CFD work is only able to capture laminar flow, a general trend of loop velocity at high power can be qualitatively found by using the uniform velocity profile at the end of the evaporator section.

The results for NCG tube Designs #2 and #2B are shown in Figure 18 with the reduced condensation rate. For Design #2 (see Figure 18(a)) the CFD and experimental results agree very well. The test for Design #2 covers a relatively low power range. For Design #2B (see Figure 18(b)), the agreement is reasonable up to about 130W, as in the case of Design #1. Although the smaller diameter part of Design #2B has a slightly larger inner diameter than Design #2, the loop velocity is not significantly influenced by this difference.

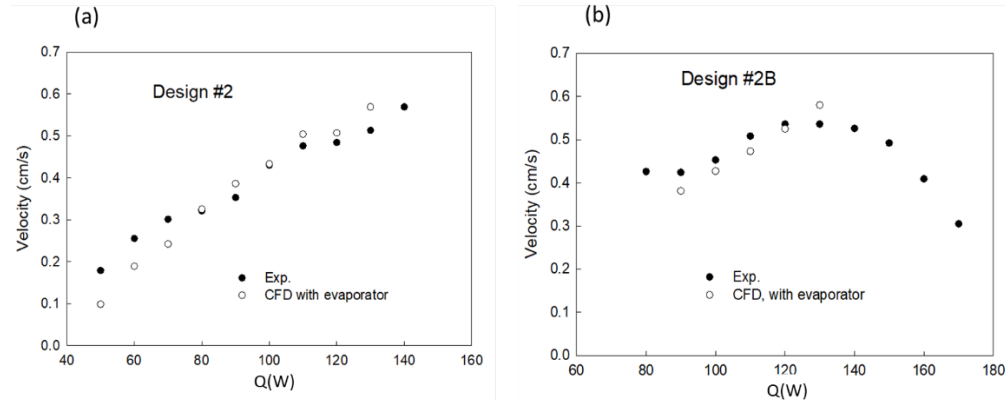


**Figure 18. Comparison of induced flow velocity between CFD and experiment results (a) with NCG tube Design #2 (b) with NCG tube Design #2B**

## V. Conclusion

A novel HR-VCHP configuration was developed where an additional NCG tube connects the end of the condenser with the reservoir forming a loop. The purpose of adopting this loop configuration was to improve fluid management within the VCHP. Based on both experimental and numerical investigation, a net NCG flow can be induced by the momentum exchange between vapor and NCG within the VCHP portion of the loop. A systematic study on momentum-induced flow was performed through both experiment and CFD analysis. Two NCG tube designs were tested on a loop VCHP experimental setup. It was observed from the experiment that:

- (1) The measured momentum-induced flow velocity is 0.5 cm/s. With this flow, VCHP purging time can be significantly reduced (from days to an hour).
- (2) The momentum induced flow rate is influenced by internal NCG tube geometry (length, diameter)
- (3) Reducing the internal NCG tube OD is favorable for flow generation
- (4) Keeping the NCG tube exit away from the vapor-NCG interface is also favorable for flow generation
- (5) With the NCG flow, the NCG humidity in the reservoir can be maintained constant and so the vapor temperature/pressure.

A CFD model was developed to study the flow behavior within the VCHP. Vapor flow velocity and pressure distribution within the heat pipe section were calculated. It was found that a recirculation vortex forming behind the internal NCG tube outlet would significantly alter the flow fields as well as the pressure distribution along the axial direction, which will impact the momentum-induced flow rate through the loop. The CFD results match well with the experimental data for all three different NCG tube designs that were investigated.

As next steps, ACT will develop an HR-VCHP prototype with a relevant geometry and tested it in simulated relevant conditions. CWRU will utilize the validated CFD model to investigate the gravity effect. Also, the model will be utilized to test relevant working fluids (ammonia and propylene) and validate the results with experimental data conducted at ACT. Predictions on the performance of the HR-VCHP prototype operating on the moon surface will be performed as well. The relationship between induced flow and purging capability will be studied through experiment and modeling.

## Appendix

Governing equations to solve axisymmetric and incompressible flow within the VCHP domain are as follows:

$$\text{Continuity Equation} \quad \frac{1}{r} \frac{\partial(ru_r)}{\partial r} + \frac{\partial(u_z)}{\partial z} = 0 \quad (1)$$

$$\text{Condensation BC} \quad \dot{m}_{cond} = \frac{h_c A_c (T_{sat} - T_{sink})}{h_{fg}} \quad (2)$$

$$\text{r- Momentum Equation (radial)} \quad \rho \left( u_r \frac{\partial u_r}{\partial r} + u_z \frac{\partial u_r}{\partial z} \right) = -\frac{\partial P}{\partial r} + \mu \left[ \frac{1}{r} \frac{\partial}{\partial r} \left( r \frac{\partial u_r}{\partial r} \right) - \frac{u_r}{r^2} + \frac{\partial^2 u_r}{\partial z^2} \right] \quad (3)$$

$$\text{z- Momentum Equation (axial)} \quad \rho \left( u_r \frac{\partial u_z}{\partial r} + u_z \frac{\partial u_z}{\partial z} \right) = -\frac{\partial P}{\partial z} - \rho g \sin \varphi + \mu \left[ \frac{1}{r} \frac{\partial}{\partial r} \left( r \frac{\partial u_z}{\partial r} \right) + \frac{\partial^2 u_z}{\partial z^2} \right] \quad (4)$$

$$\text{Energy Equation} \quad \frac{\partial T}{\partial t} = \alpha \nabla^2 T \quad (5)$$

$$\text{Diffusion Equation} \quad \frac{\partial \phi}{\partial t} = D_{12} \nabla^2 \phi \quad (6)$$

## Acknowledgments

This project is sponsored by NASA Marshall Space Flight Center (MSFC) under an STTR Phase II program (Contract# 80NSSC20C0023) and Phase I program (Contract# 80NSSC18P2155). We would like to thank the program manager, Brian O'Conner, and Dr. Jeff Farmer for their support and valuable discussions during the program. In addition, special appreciation goes to Chris Jarmoski and Philip Texter who have provided significant technical contributions to this project.

## References

- 
- <sup>1</sup> Tarau C., Schwendeman C. L., Schifer N.A., Polak J. and Anderson W.G., "Optimized Back up Cooling System for the Advanced Stirling Radioisotope Generator", in *International Energy Conversion Engineering Conference (IECEC)*, 2015
  - <sup>2</sup> Tarau C., Schwendeman C.L., Anderson W.G., Cornell P.A. and Schifer N.A., "Variable Conductance Heat Pipe Operated with Stirling Converter", in *IECEC, 2013*
  - <sup>3</sup> Tarau C. and Anderson W.G., "Variable Conductance Thermal Management System for Balloon Payload", in *20th AIAA Ligher-Than-Air Systems Technology Conference*, 2013
  - <sup>4</sup> Tarau C., Ababneh M.T., Anderson W.G., Alvarez-Hernandez A.R., Ortega S., Farmer J.T. and Hawkins R., "Advanced Passive Thermal eXperiment (APT<sub>x</sub>) for Warm-Reservoir Hybrid-Wick Variable Conductance Heat Pipes on the International Space Station (ISS)" in *48th International Conference on Environmental Systems (ICES)*, 2018
  - <sup>5</sup> Lee K-L., Tarau C., Lutz A., Anderson W.G., Huang C-N., Kharangate C. and Kamotani Y., "Advanced Hot Reservoir Variable Conductance Heat Pipes for Planetary Landers", in *50th International Conference on Environmental Systems (ICES)*, 2020